Monomer adds to preformed structured oligomers of Abeta-peptides by a two-stage dock-lock mechanism

Phuong H. Nguyen, Mai Suan Li, Gerhard Stock, John E. Straub, and D. Thirumalai

PNAS 2007;104;111-116; originally published online Dec 26, 2006;
doi:10.1073/pnas.0607440104

Monomer adds to preformed structured oligomers of Aβ-peptides by a two-stage dock–lock mechanism

Phuong H. Nguyen*, Mai Suan Li[†‡], Gerhard Stock*, John E. Straub[§], and D. Thirumalai[‡¶‖]

*Institute of Physical and Theoretical Chemistry, J. W. Goethe University, Marie-Curie-Strasse 11, D-60439 Frankfurt, Germany; [†]Institute of Physics, Polish Academy of Sciences, Al. Lotnikow 32/46, 02-668 Warsaw, Poland; [§]Department of Chemistry, Boston University, Boston, MA 02215; and [¶]Biophysics Program, Institute for Physical Science and Technology, and [‖]Department of Chemistry and Biochemistry, University of Maryland, College Park, MD 20742

Edited by Harold A. Scheraga, Cornell University, Ithaca, NY, and approved November 3, 2006 (received for review August 25, 2006)

Nonfibrillar soluble oligomers, which are intermediates in the transition from monomers to amyloid fibrils, may be the toxic species in Alzheimer's disease. To monitor the early events that direct assembly of amyloidogenic peptides we probe the dynamics of formation of $(A\beta_{16-22})_n$ by adding a monomer to a preformed $(A\beta_{16-22})_{n-1}$ ($n = 4-6$) oligomer in which the peptides are arranged in an antiparallel β-sheet conformation. All atom molecular dynamics simulations in water and multiple long trajectories, for a cumulative time of 6.9 μs, show that the oligomer grows by a two-stage dock–lock mechanism. The largest conformational change in the added disordered monomer occurs during the rapid ($\approx$50 ns) first dock stage in which the β-strand content of the monomer increases substantially from a low initial value. In the second slow-lock phase, the monomer rearranges to form in register antiparallel structures. Surprisingly, the mobile structured oligomers undergo large conformational changes in order to accommodate the added monomer. The time needed to incorporate the monomer into the fluid-like oligomer grows even when $n = 6$, which suggests that the critical nucleus size must exceed six. Stable antiparallel structure formation exceeds hundreds of nanoseconds even though frequent interpeptide collisions occur at elevated monomer concentrations used in the simulations. The dock–lock mechanism should be a generic mechanism for growth of oligomers of amyloidogenic peptides.

There is intense interest in determining the structures, kinetics, and growth mechanisms of amyloid fibrils (1–8) because they are associated with a number of diseases such as Alzheimer's (9) and Parkinson's (6) disease as well as prion pathology (10). Recently, significant progress has been made in determining the structures of amyloid fibrils (1, 11–13). The structures of fibrils of a number of peptides including Aβ_{1-40} and Aβ_{1-42} that have been proposed using constraints obtained from solid state NMR (13) are also consistent with molecular dynamics simulations (14). In addition, a high resolution crystal structure of peptides extracted from N-terminal segments of Sup35 has been recently reported (15). These studies have confirmed that many peptides, which are unrelated by sequence, adopt the characteristic cross β-pattern in the fibril state.

It is also important to understand the mechanisms of their formation starting from monomers because it is becoming increasingly clear that the nonfibrillar intermediates may be the toxic species in at least the Alzheimer's disease (9). Experimental characterization of the mechanism of formation of oligomers and their structures is difficult because of their diverse morphologies and rapid conformational fluctuations (16–19). Molecular dynamics (MD) simulations (14, 16, 20) can not only identify the interactions that drive the oligomer formation, but also can provide a molecular picture of the dynamics of the early events in the route to amyloid fibrils (16).

In a previous study, we investigated the factors that govern the assembly mechanism of trimers of Aβ_{16-22} peptides (16). Following our initial work and a related study on trimers of a fragment from Sup35 (19), a large number of computational papers have focused on various aspects of oligomer formation and fibrils (17, 18, 21–24). The computational studies on the soluble dynamically fluctuating oligomers have elucidated the importance of side chains (and hence the sequence) in directing the aggregation process (16, 19). Here, we probe the mechanism of how structured oligomers grow upon addition of an unstructured monomer. The kinetics of addition of soluble Aβ monomers to preformed fibril structures has been investigated experimentally (25, 26) and using theoretical arguments (27). These important studies showed that the association of monomers to the amyloid fibril occurs by multistep kinetics, based on which it was proposed that fibril elongation occurs by a dock-lock mechanism (25, 26). A similar mechanism may be operative in the growth of the Sup35 amyloid, which occurs by addition of a single monomer to a growing end of a fibril (3). In these templated-assembly studies (3, 25, 26), it is unlikely that the fibrils themselves undergo substantial conformational changes. In contrast, because the oligomers are highly dynamic, it is unclear how a preperformed oligomer interacts with a nascent monomer.

To probe the dynamics of oligomer growth, we investigated the assembly mechanism of

$$(A\beta_{16-22})_{n-1} + A\beta_{16-22} \rightleftharpoons (A\beta_{16-22})_n, \quad n = 4, 5, 6, \qquad [1]$$

using extensive molecular dynamics simulations in explicit water (*Methods*). Monomer adds to the structured oligomer by a two-phase dock–lock mechanism (25, 26). In the first rapid dock phase, the unstructured Aβ_{16-22} docks onto a preformed oligomer. In the second (lock) step, interaction of the monomer with the "fluid-like template" results in substantial conformational changes. Surprisingly, in the lock phase, the preformed oligomer itself dynamically fluctuates to accommodate the monomer. The rate-determining step in the monomer addition is the lock phase in which combined conformational changes that both the preformed oligomer and the monomer undergo to form a stable antiparallel higher order oligomer. The lock phase is sufficiently slow that, even at the very high peptide concentrations used in the simulations, we did not observe fully antiparallel structures for $n = 6$, after hundreds-of-nanoseconds simulations. Water molecules are expelled early in the assembly process, thus making the interior of the ordered oligomers dry. Because the biophysical basis of the oligomer assembly mechanism is general, we suggest that growth of other amyloidogenic peptides might also follow the dock–lock mechanism. The oligomers grow by addition of one monomer at a time, and hence the dock–lock mechanism is independent of the monomer concentration (3).

Author contributions: M.S.L., J.E.S., and D.T. designed research; P.H.N. and M.S.L. performed research; G.S. contributed new reagents/analytic tools; P.H.N., M.S.L., and D.T. analyzed data; and M.S.L. and D.T. wrote the paper.

The authors declare no conflict of interest.

This article is a PNAS direct submission.

[‡]To whom correspondence may be addressed. E-mail: masli@ifpan.edu.pl or thirum@glue.umd.edu.

This article contains supporting information online at www.pnas.org/cgi/content/full/0607440104/DC1.

Results and Discussion

Monomers Fluctuate Between a Number of Rapidly Interconverting Minima. An important goal of this work is to determine the conformational changes that the monomer undergoes upon interacting with a preformed oligomer. As a first step, we have characterized the relevant minima that are sampled by the monomer during the 0.36-μs simulations. The monomer adopts predominantly flexible random coil conformations (≈65%). The β-strand content is ≈10%, whereas the α-helix is ≈25%. Comparison with our earlier study (16) shows that, regardless of the force field, $A\beta_{16-22}$ monomer predominantly adopts a random coil conformation. From the the free-energy profile expressed in terms of the first two principal components, we find that [see supporting information (SI) Fig. 6] $A\beta_{16-22}$ samples a number of minima that are separated by small free-energy barriers (<1 kcal/mol).

The Antiparallel $(A\beta_{16-22})_3$ Is Mobile. The simulations of the trimers were initiated by placing the three peptides in random orientations. Upon interpeptide interaction, the ordered $(A\beta_{16-22})_3$ structures form. The energy of $(A\beta_{16-22})_3$ is lower than that of three isolated monomers (Fig. 1*a*), which implies that the oligomer conformation is more favorable than the three noninteracting peptides. At long times, $(A\beta_{16-22})_3$ forms antiparallel β-sheet structures in which the backbone of each of the monomers is in a plane (Fig. 1*b*). However, because of the finite size effects, the ordered oligomers are only marginally stable. As a result of conformational fluctuations, $(A\beta_{16-22})_3$ samples, a number of alternative structures (Fig. 1*b*) that are separated from the dominant minima by small free energy barriers. The nematic liquid crystalline order parameter $\langle P_2 \rangle$, which gives the overall orientation of the peptides with respect to a director, is ≈0.5 for the most populated minimum. There are other basins (Fig. 1*b*) in which $\langle P_2 \rangle$ is relatively high, which suggests a high degree of orientational order (due to antiparallel arrangement of the peptides) in the higher free-energy minima. Fig. 1*b* shows that, although antiparallel structures are the most stable, they interconvert among other competing basins of attraction on the time scale of simulations (between ≈100 and/or 680 ns). The large conformational fluctuations are also reflected in the dynamics of P_2 (Fig. 2*a*) and the shallow barrier separating ordered and disordered arrangement of the $A\beta_{16-22}$ peptides (see Fig. 2*a* Inset).

Peptide Association Occurs with High Probability from Unfolded Monomer Conformations. If we set the first time $P_2 \approx 0.9$ (corresponding to the location of the second minimum in the free energy as a function of P_2 Fig. 2*a Inset*) as the first passage time for antiparallel assembly ($\tau_{APA,i}$) in the ith trajectory, we find that $\tau_{APA,i}$ ranges from ≈7 to 600 ns depending on i. The long value of $\tau_{APA,i}$ for $i = 5$ (Fig. 2*b*) illustrates the role that the initial conformations of the peptides play in the mechanism of assembly. In the fifth trajectory, the initial conformation of the one of the peptides is in a random coil state, whereas peptide 2 has a turn and peptide 3 is in a α-helical state. The starting structures for the peptides in all other trajectories are random coils. The value of $\tau_{APA,5}$ (Fig. 2*b*) that exceeds 600 ns, compared to the much smaller values for other trajectories (see Fig. 2*a* for an example), shows that oligomers form rapidly if during the initial collision the contact radius is as large as possible, which is most probable if the peptides are in the random coil state. From this result, we also conclude that, if any of the peptides is in an ordered state, then it has to at least partially unfold to facilitate oligomerization. The multiplicity of routes in the trimer formation, which is reflected in the role the initial structure plays in the oligomerization process, is consistent with pathway diversity observed in the aggregation of proteins using lattice models (28). It was also shown in ref. 28 that the most efficient kinetic assembly occurs if the associating monomers are unfolded and random coil-like because such conformations maximize the interpeptide contact radius. Alternatively, it is likely that a monomer in the helical conformation can easily add to the oligomer as a random-coil conformation. However, the reorganization of the helical structure is far less probable.

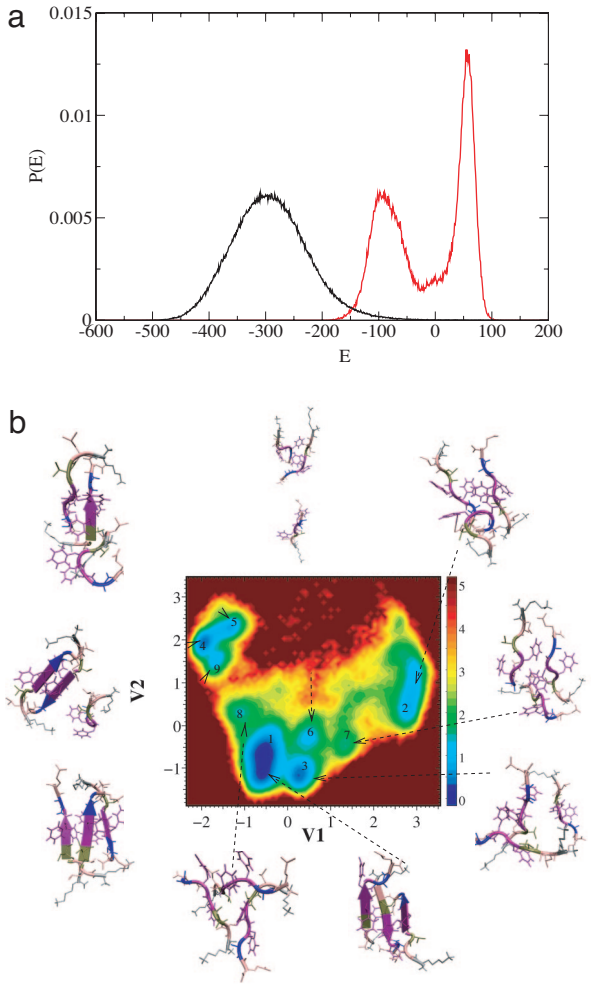

Fig. 1. Energy landscape of $(A\beta_{16-22})_3$. (*a*) Distribution of energies (in kcal/mol) for the $(A\beta_{16-22})_3$ (black) and the monomer (red). The energy represents the total energy of the system including water molecules. The low-energy monomer peak corresponds to random coil conformations, whereas the higher energy represents extended states. (*b*) Projection of the free energy surface for $(A\beta_{16-22})_3$ in terms of the lowest two eigen vectors of the dPCA (see *Methods*). The scale for the free energy (in kcal/mol) is given on the right. The structure in the most populated basin corresponds to the peptides that are arranged in an antiparallel manner.

Estimation of Oligomerization Time Scale. The peptide concentration, which is on the order of 100 μM under *in vitro* fibril growth conditions (13), is in the ≈40–70 mM range (Table 1) in our simulations. As a result, the interpeptide collision probability is greatly enhanced which naturally would lead to smaller times for forming ordered structures. In principle, the formation time of ordered trimer starting from monomers can be computed using $\tau_{APA,i}$ for a number of trajectories. This is, at present, not possible given that a large number of independent trajectories are required to obtain reliable values for the mean passage time. From the five trajectories, we estimate that the mean time $\langle \tau_{APA} \rangle \approx 244$ ns. In order to supplement this estimate we have also calculated $\langle \tau_{APA} \rangle$ by assuming that association occurs by a diffusive motion in a free-energy profile (29). Using P_2 as an appropriate one-dimensional

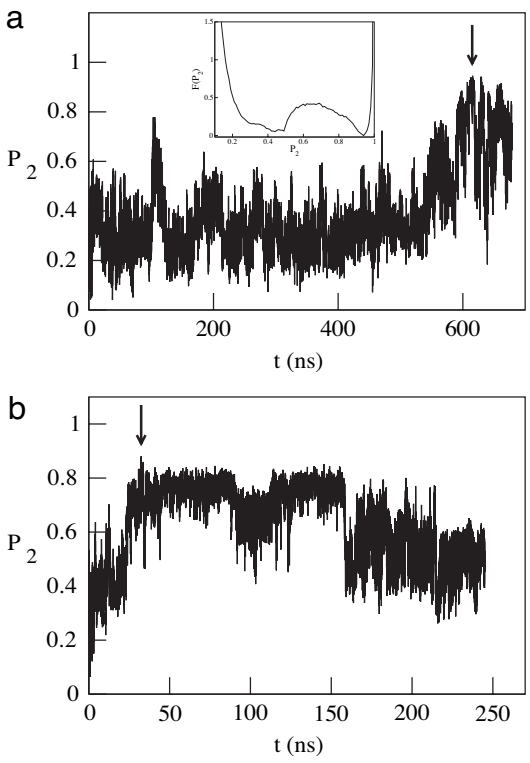

Fig. 2. Time dependence of P_2. (*a*) Dynamics of fluctuation the global orientational order parameter that characterizes the oligomer. Here, $P_2(t)$ for the assembly of three $A\beta_{16-22}$ peptides as a function of t is shown for a trajectory labeled 5 (see Table 1). The starting structures of the monomers for this trajectory is different from those in the other trajectories. Even on extremely long simulation times, the value of P_2 remains less than in other trajectories in which the initial conformations of the peptides were in random coin states. (*Inset*) The free energy (in units of kcal/mol) profile as a function of P_2. The highly ordered basin of attraction centered at $P_2 \approx 0.9$ is separated from the ensemble of disordered oligomers by a modest free-energy barrier. (*b*) Time dependence of P_2 for a trajectory in which a highly ordered trimer form a very rapidly. The first passage time for antiparallel structure for this trajectory is $\tau_{APA,i} \approx 40$ ns (indicated by an arrow). There are substantial fluctuations after ordered assembly which shows that the antiparallel $(A\beta_{16-22})_3$ is only marginally stable.

reaction coordinate (see the free-energy profile in Fig. 2*a Inset*) $\langle\tau_{APA}\rangle$ is calculated by using

$$\langle\tau_{APA}\rangle = \frac{1}{D}\int_{P_{2D}}^{P_{2AP}} dP_2 \int_0^{P_2} dP_2' \exp\{\beta[\Delta G(P_2) - \Delta G(P_2')]\}, \quad [2]$$

Table 1. Simulation details

	Duration, ns				
Trajectory	Monomer	Trimer	Tetramer	Pentamer	Hexamer
1	360	233	224	360	330
2	—	145	240	540	805
3	—	245	400	737	457
4	—	70	600	329	514
5	—	680*	—	—	—
Volume†	43 (39)‡	78 (64)	117 (57)	128 (65)	174 (57)

*The initial conformation of the three peptides correspond to coil, turn, and helical structures.
†Volume of the cubic box is given in nm^3.
‡The numbers in parenthesis are peptide concentrations in mM.

where D is a characteristic diffusion time, $\Delta G(P_2)$ is the free-energy profile as a function of P_2, P_{2D} ($\approx$0.4) and P_{2AP} ($\approx$0.9) are the mean values of P_2 in the disordered and ordered states of the trimer, and $\beta = 1/k_BT$. If we approximate $\Delta G(P_2)$ by a parabolic well around P_{2D} and P_{2AP}, then $D(P_2)$ may be approximated as $D(P_2) = (\Delta P_2)^2/\tau_{corr}$, F, where $(\Delta P_2)^2$ and τ_{corr} are the variance and autocorrelation time of the reaction coordinate P_2, respectively. From the kinetic data for P_2 in the five trajectories, we estimate $\tau_{corr} \approx 0.25$ ns, $(\Delta P_2)^2 \approx 0.002$, and $D(P_2) \approx 0.008$ ns^{-1}. Using these values in Eq. **2**, we obtain $\langle\tau_{AP}\rangle \approx 220$ ns. Given the approximation used in computing $\langle\tau_{AP}\rangle$ in Eq. **2**, the agreement with the rough estimate from simulation is good.

Antiparallel Order Increases as the Oligomer Size Grows. By monitoring the energies and other structural features (β-strand content of the peptides and P_2), we find that the oligomer, in which the peptides are extended compared to the monomer conformations, forms with high probability at long times. From the free-energy profiles, we find that the number of minima decreases as one goes from trimer to higher-order oligomers (compare Figs. 1*b* and 3*a*). Concomitantly, the β-strand content of the peptides increases as well. For example, the probability of being in the antiparallel structure with high β-strand content in each of the peptides increases from $\approx$30% in the trimer to $\approx$60% in the hexamer. In both the pentamer and the hexamer, the antiparallel structure is the most stable. The structures in many of the minima that are not the most populated also have antiparallel arrangement of the peptides. Thus, the ordered oligomer in which the peptides are arranged in antiparallel manner becomes increasingly stable as its size grows. However, the transition to a stable ordered state with high value of P_2 occurs only on long time scales (Fig. 3*b*). From SI Fig. 7, it is clear that $(A\beta_{16-22})_3$ does form stable antiparallel with $P_2 \approx 0.9$.

Interpeptide Side-Chain Interactions Stabilize Antiparallel Structures. In order to probe the interactions that stabilize the ordered oligomers we calculated the contacts between the side chains of the added monomer to one of the peptides of the preformed oligomer. Fig. 4 *a* and *c* shows, for the tetramer and the pentamer, respectively, that the contacts between the stability arises due to a number of interpeptide contacts between the hydrophobic residues of the central hydrophobic cluster (CHC). As expected the antiparallel orientation is guaranteed by the formation of the salt bridge between K16 from one peptide and E22 from another. In contrast, there are very few stable hydrogen bonds that persist between the peptides (Fig. 4 *b* and *d*). Stable hydrogen bonds are likely to be found only when the oligomer size exceeds the critical nucleus of when there are several β-sheet layers. The interpeptide hydrogen bonds fluctuate and therefore do not contribute significantly to the overall stability of the oligomer. Taken together, these results show that the driving force for oligomerization is the favorable interpeptide association between residues belonging to the CHC.

Preformed Oligomers Undergo Conformational Fluctuations to Accommodate the Added Monomer. To probe the mechanism of growth of oligomers we added one monomer at a time to a preformed oligomer in which the peptides are arranged in antiparallel manner with a high value of P_2. We used P_2 as a global order parameter to monitor the overall time-dependent fluctuations in the preformed and growing oligomer. For one of the trajectories, $P_2(t)$ for the tetramer and the preformed trimer, from which it is formed, shows that, even on time scales that exceed 200 ns, P_2 fluctuates greatly (Fig. 3 *b* and *c*). Although the initial value of P_2 for the trimer is $\approx$0.8, we find that during the growth process it becomes as low as 0.2 (Fig. 3*b*). On times longer than $\approx$300 ns, the tetramer is ordered with P_2 fluctuating around 0.8. Similar behavior is found in P_2 for addition of a monomer to preformed tetramer and pentamer as well (SI Fig. 8).

Although the overall time dependence of $P_2(t)$ is qualitatively

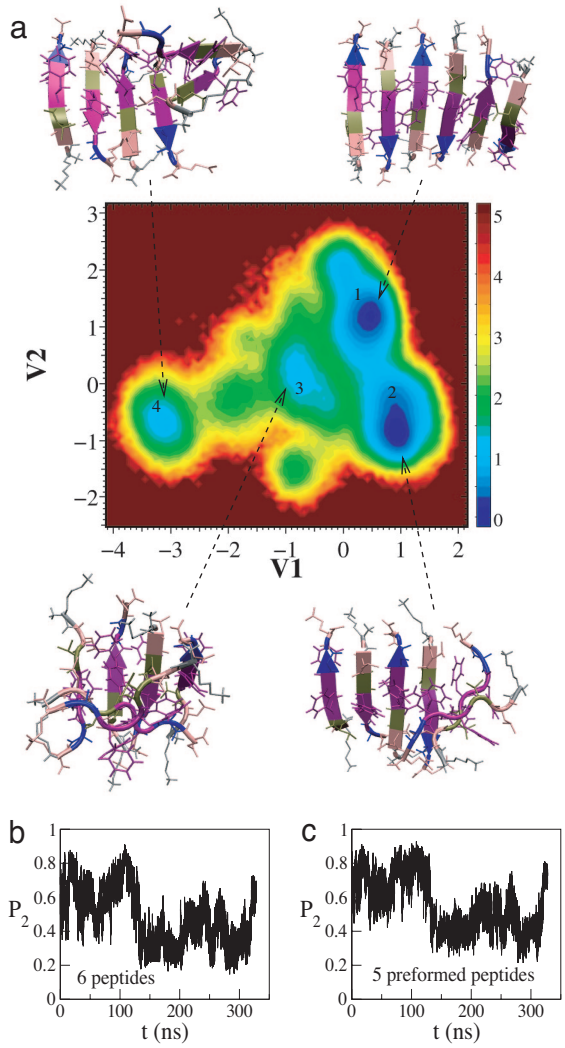

Fig. 3. Free energies and dynamics for the hexamer. (*a*) Free-energy diagram projected onto the first two principal components V_1 and V_2 of the dPCA for the hexamer. The free-energy scale is given on the right. The structure in the basin labeled 1 shows that the monomers arranged in antiparallel fashion. The energy-minimized structures from the second basin would also correspond to an ordered hexamer. The presence of other minima could potentially act as kinetic traps that delay oligomerization. (*b*) Time dependence of P_2 for one of the trajectories. This curve monitors the changes in the order parameter upon monomer addition. The initial value of P_2 for the pentamer exceeds 0.8, which implies shortly (<1 ns) the added monomer induces fluctuations in the structured oligomer. (*c*) Dynamics of P_2 for the structured pentamer that roughly mirrors *a*. The large fluctuations shows that the initially ordered pentamer orientationally melts (disorders) to accommodate the added monomer.

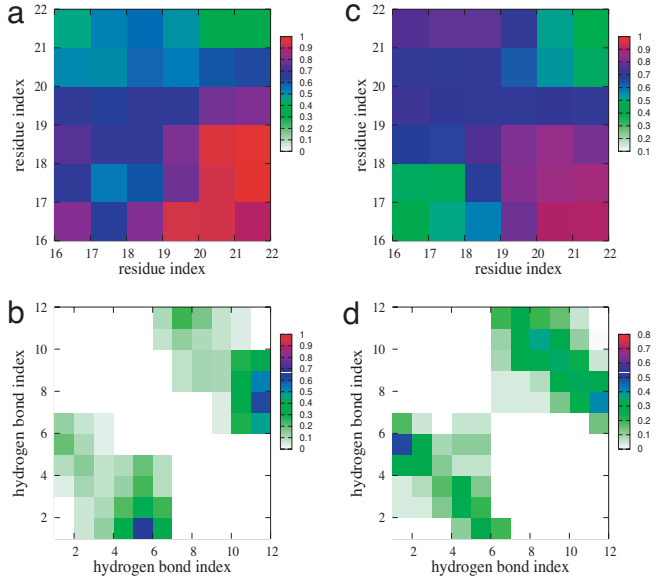

Fig. 4. Side chain contacts and interpeptide hydrogen bonds. (*a*) Color-coded graph showing the contacts between side chains of the added monomer to a preformed trimer. The contacts are obtained by averaging over time and the trajectories. The scale on the right gives the extent of formation of a specific contact. Contacts that form with high probability are those between the residues in the central hydrophobic cluster and the interpeptide salt bridge. (*b*) Probability of formation of interpeptide hydrogen bonds. The scale on the right gives the probability of hydrogen bond formation. Clearly, there are very few hydrogen bonds that persist in stabilizing the oligomer. (*c*) Same as *a* except it is for a pentamer. (*d*) Same as *b* except it is for a pentamer.

similar for all the oligomers, the fluctuations in P_2 decreases as the oligomer size increases. We have quantified the dependence in the order parameter fluctuations on the oligomer size using $\Delta P_2 = \sqrt{\langle P_2^2\rangle - \langle P_2\rangle^2}$, where $\langle \ldots \rangle$ refers to the time average over all trajectories. We find that ΔP_2 is largest for the trimer ($\approx$0.22) and decreases as the oligomer size increases reaching $\Delta P_2 \approx 0.12$ in the hexamer.

Monomers Add by a Dock–Lock Mechanism. To show that the added monomer is incorporated into the preformed oligomer by a two-stage dock–lock mechanism, we followed the dynamics of contact formation between the side chains of the nascent monomer and those of the oligomer as well as the growth in the β-strand content of the peptides. For clarity, we present results for the reaction $(A\beta_{16-22})_5 + A\beta_{16-22} \Rightarrow (A\beta_{16-22})_6$. In the absence of interaction with the oligomer, the probability of being in the β-strand conformation is $\approx$0.1. In addition, the monomer is in a relatively compact state whereas interaction with the oligomer leads to extension of the chain and an increase in the β-strand content. The dynamic changes in the β-strand content are monitored using $\beta(t) = 1/N_T \sum_{i=1}^{N_T} 1/\Delta \sum_t^{t+\Delta} \beta_i(s)ds$, where N_T is the number of trajectories, and $\beta_i(s)$ is the instantaneous strand content of the monomer or the oligomer. To filter the high-frequency noise, the instantaneous values of $\beta_i(s)$ are averaged over an interval $\Delta = 1$ ns. Fig. 5*a* shows that the high initial β-strand content of the oligomer is maintained during the course of the simulation. The β-strand content of the added monomer grows in stages. In the first phase, the β-strand content increases substantially from its initial value. Fig. 5*a Inset* shows that most of the growth occurs immediately upon docking. Within 1 ns after interaction with the hexamer, the β-strand content of the added monomer increases to $\approx$0.3 (Fig. 5*a*). The extent of strand formation continues to increase over a period of tens of ns and fluctuates around 0.65 for $\approx$100 ns. During this initial docking stage, there are large changes in the structure of the nascent monomer. Given that the monomer is a small peptide, there is a relatively sharp transition that defines the locking stage, in which the β-strand content of the added monomer approaches that of the preformed pentamer. In this trajectory, the average β-strand content of the peptides in the pentamer fluctuates around 0.8.

To illustrate the dynamics of approach of the β-strand content of the added monomer to the value expected in the hexamer (roughly that of the structured pentamer), we have computed $\bar{\beta}(t) = 1/N_T \sum_{i=1}^{N_T} 1/t \sum_0^t \beta_i(s)ds$, which is the running time average of the strand content averaged over N_T trajectories. If the added monomer is fully incorporated into the preformed oligomer, then $\beta(t)$, at long times, would approach the equilibrium value. From the dynamics of $\bar{\beta}(t)$ (Fig. 5*b*), we find that for $t < 50$ ns (the docking stage) the strand

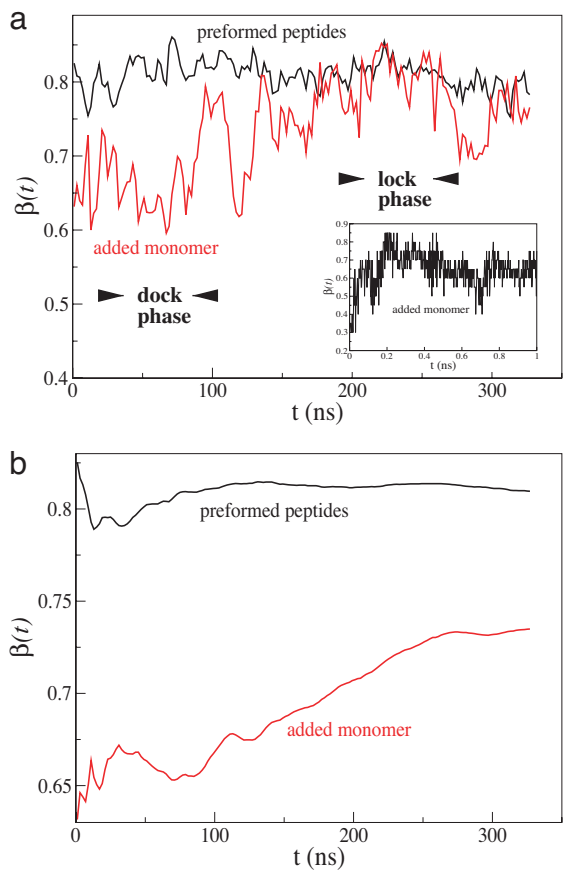

Fig. 5. Probes of lock–dock mechanisms. (*a*) Average (over the four trajectories listed in Table 1) value of the dependence of the β-strand content for the preformed pentamer and the added monomer as a function of time. The value of $\beta(t)$ for the structured oligomer remains high and fluctuates around its initial value of $\beta \approx 0.8$. The β-strand content of the added monomer is considerably less than that of the structured pentamer for $t < 120$ ns that roughly corresponds to the dock phase. For $t > 120$ ns, which represents the lock phase, the β-strand content coincides with the value in the ordered state. (*Inset*) The changes in the β-strand of the monomer for $t \leq 1$ ns. It is clear that the maximum change in the extent of β-strand conformation occurs immediately upon docking. (*b*) Dynamics of approach of the running time average and over the trajectories of the β-strand values of the pentamer and the added peptide. Long after the dock phase the value of $\bar{\beta}(t)$ of the monomer has not reached the asymptotic value ($\bar{\beta} \approx 0.8$), which shows that the lock phase is kinetically slow.

content increases from its low monomeric value to $\beta \approx 0.8$. Thus, most of the fast conformational change in the monomer occurs in the initial phase. For $t > 100$ ns, which corresponds to the lock phase, the strand content of the monomer continues to increase, albeit very slowly. Indeed, the addition of a monomer to a pentamer with well formed initial β-sheet is not complete even at $t \approx 300$ ns. The simulations show that the time scale for the lock stage is considerably longer than for the dock phase. The large separation in the rates of the dock and lock phases is consistent with experimental findings that have probed the kinetics of addition of a monomer to the ends of a fibril (25, 26). It appears that, in the growth of the fibrils and prenucleus oligomers, the rate-limiting step is the locking phase.

The results in Fig. 5 show that, both collectively and individually, the $A\beta_{16-22}$ peptides have a large β-strand content. On the other hand, preformed structures undergo substantial variations in the global order parameter P_2 (Figs. 3 and 4). From the results in Figs. 3–5, we infer that, to accommodate the added monomer, the rest of the structured oligomer undergoes largely orientational disordering, leading to a decrease in P_2, without sacrificing the extent of strand formation in the individual peptides. Our inference is substantiated by the dynamics of orientational disordering $P_1^i = \langle \vec{u}_i(0) \cdot \vec{u}_i(t) \rangle$, where $\vec{u}_i$ is the unit vector that joins the N and C atoms of the C and N termini of the ith peptide. SI Fig. 9 shows that $P_1^i(t)$ decays rapidly, which implies that there is considerable orientational rearrangement within the oligomer. These results imply that the mobility of the oligomers arises largely from the internal orientational freedom of the individual peptides.

Relaxation Time of the Monomer Depends on the Oligomer Size. The present work shows that, upon addition of the nascent monomer, the preformed oligomer also undergoes conformational rearrangement. Because reconfiguration time scales increase as the oligomer size increases, we expect that the time needed for a monomer to be incorporated, τ_{inc}, should increase as n (Eq. **1**) increases. Once the critical nucleus is reached, τ_{inc} should become independent of n. Although we do not have enough trajectories we have obtained approximate values of τ_{inc} for all $n = 4$, 5, and 6. Assuming that τ_{inc} is the mean time for the $P_2 \approx 0.9$ for the oligomer, we find that $\tau_{inc} \approx$ 23 ns for the trimer, i.e., the newly added monomer, is incorporated into the preformed trimer in ≈23 ns. For $n = 4$, we estimate $\tau_{inc} \approx$ 114 ns, whereas for $n = 5$, we speculate that τ_{inc} exceeds 220 ns. The increasing values of τ_{inc} as n increases further reinforces the notion that even the hexamer is not the critical nucleus.

Conclusion

We have carried out extensive molecular dynamics simulations of the oligomerization process for the $A\beta_{16-22}$ trimer, tetramer, pentamer, and hexamer to decipher the mechanism by which an added monomer is incorporated into a well defined preformed oligomer. For all of the systems studied, we observed the formation of ordered antiparallel β-sheet structures that mimic the conformations adopted in the fibril state. The antiparallel $(A\beta_{16-22})_n$ ($n = 3$–6) structures, which form only on long time scales, are dynamic. Because of the presence of a number of alternate structures, kinetic trapping in the oligomerization process is a common occurrence.

In the process of accommodating the monomer, the preformed structured oligomer with high average β-sheet content undergoes large fluctuations in P_2 that are linked to orientational disordering of the individual peptides. Fluctuations would be smaller if n exceeds the size of the critical nucleus n_c. Because even the hexamers are dynamic, we infer that the size of the critical nucleus exceeds six. Further evidence that n_c must be greater than six comes from our observation the estimated time needed for adding a monomer to the oligomer increases with n. The values of τ_{inc} should become approximately independent of n if $n > n_c$.

Of particular importance is the conclusion that, upon adding a disordered monomer to an ordered oligomer, growth occurs largely by a two phase dock–lock mechanism. The maximum change in the conformation of the added monomer occurs during the rapid dock phase whereas in the much slower lock phase, the monomer forms a β-strand that is in registry with the rest of the oligomer. Somewhat surprisingly, the initial ordered oligomer partially disorders in order to accommodate the monomer. Because the time scale for the transient disordering process increases as n increases, we find that τ_{inc} also increases with n.

The mechanistic features of the dock–lock mechanism discovered here for the oligomer growth are qualitatively similar to the carefully documented steps in the fibril elongation kinetics by Esler *et al.* (26) and Cannon *et al.* (25). In both cases, the rate-limiting step appears to be the lock phase in which the monomer adopts in register parallel for $A\beta_{1-40}$ peptides and antiparallel for the $A\beta_{16-22}$ peptides. There is an important difference between the mechanism governing fibril elongation and oligomer growth. In the former case, the fibril is a template that does not fluctuate. In contrast, in the oligomer growth process, the monomers belonging to the

oligomer and the added monomer may repeatedly associate and disassociate before forming a stable ordered structure. In this sense, the fluid dock–lock mechanism for oligomer growth is reminiscent of the transient binding and release (TBR) process that is operative in the assisted folding of proteins and RNA (30, 31). The TBR might explain the sluggish times scale of the the lock phase.

Methods

Initial Oligomer Conformations. The initial conformation for the $A\beta_{16-22}$ monomer used in the simulations (for details see SI *Text*) was extracted from the structure of the $A\beta_{10-35}$ peptide available in the Protein Data Bank (ID code 1hz3) (32) (see SI Fig. 10). The ends of the monomer are capped, and the simulated sequence is Ace–Lys–Leu–Val–Phe–Phe–Ala–Glu–NH_2. The $A\beta_{16-22}$ sequence includes the LVFFA central hydrophobic cluster that is thought to drive the aggregation process in the full-length $A\beta$ peptide. The terminal residues are oppositely charged (a positive charge on lysine and a negative charge on glutamic acid). The initial conformations of the trimer were obtained by replicating the individual $A\beta_{16-22}$ structure in random orientations. To create an ordered antiparallel $(A\beta_{16-22})_3$ structure, we allowed the three peptides to interact by placing them in a cubic box at a concentration of 64 mM (Table 1) without using any constraining potential. The initial conformations for the tetramer were generated randomly by adding a monomer to a preformed ordered trimer that is found during the course of 250-ns simulations (SI Fig. 8). Similarly, the starting conformations of the pentamer and the hexamer were created by adding one peptide to the oligomers of the tetramer and pentamer, respectively (SI Fig. 8). The simulations were performed by using the GROMOS96 force field 43a1 (33) for the peptides and the simple point charge (SPC) water model (34).

Principal Component Analysis (PCA). We used the PCA to represent the conformational distribution of the $3N$-dimensional system (35–38). We used the dihedral PCA or dPCA that uniquely defines the distance in the space of periodic dihedral angles using the variables (39, 40) $q_k = \cos(\alpha_k)$, $q_{k+1} = \sin(\alpha_k)$. Here, $\alpha_k \in \{\phi_k, \psi_k\}$ and $k = 1 \ldots N-1$, with N being the number of backbone and side chain dihedral angles. The correlated internal motions are probed using the covariance matrix $\sigma_{ij} = \langle (q_i - \langle q_i \rangle)(q_j - \langle q_j \rangle) \rangle$.

The free-energy surface along the n-dimensional reaction coordinate $V = (V_1, \cdots V_n)$ (obtained by diagonalizing σ) is given by $\Delta G(V) = -k_B T[\ln P(V) - \ln P_{\max}]_i$, where $P(V)$ is the probability distribution obtained from a histogram of the MD data, $P_{\max}$ is the maximum of the distribution obtained from a histogram of the MD data, $P_{\max}$ is the maximum of the distribution, which is subtracted to ensure that $\Delta G = 0$ for the lowest free-energy minimum. We use dPCA to compute the free energy landscapes (FEL) using mainly the first two eigenvectors V_1 and V_2.

Measures Used in the Analysis of Structures. To characterize the fibril state of short peptides we used the nematic order parameter P_2 (41). In terms of the unit vector $\vec{u}_i$ linking N and C termini for the ith peptide, P_2 is

$$P_2 = \sum_{i=1}^{N} \frac{|\vec{r}^{\,i}_{NC}|}{L_i} P_2^0, \qquad [3]$$

where $P_2^0 = 1/2N \, \Sigma_{i=1}^{N} \, 3/2 \, (\vec{u}_i \vec{d})^2 - 1/2$, where $\vec{d}$ (the director) is a unit vector defining the preferred direction of alignment of the oligomer, N is the number of molecules, and $\vec{r}^{\,i}_{NC}$ is the end-to-end vector that connects two C_α atoms from the termini of the ith peptide. The end-to-end distance in the fully stretched state $L_i = (N_i - 1)a$, where N_i is a number of amino acids in ith monomer and a ($\approx$4 Å) is the distance between two consequesive C_α atoms.

It follows from Eq. **3** that $P_2^0 = 1$ if all peptides are precisely parallel or antiparallel, even if they are not fully extended. To characterize the "fibril" conformations adequately, we define P_2 as a product of P_2^0 and the factor, which is equal to 1 if all peptides are stretched and less than 1 otherwise (see Eq. **3**). If P_2 is bigger than 0.5, then the system has the propensity to be in an ordered state.

We have also monitored the time evolution of the formation of the side chain–side chain (SC–SC) contacts and the hydrogen bond (HB) contacts. A SC–SC contact is formed if the distance between the centers of mass of two residues is $\leq$6 Å. A HB contact is formed if the distance between donor D (or atom N) and acceptor A (or atom O) is $\leq$3.5 Å and the angle D–H–A is $\geq$135°. The β-strand, α-helical, and random-coil contents in of the peptides are calculated by using the method described in ref. 16.

This work was supported by National Institutes of Health Grant R01 GM076688-05 and Polish Komitet Badan Naukowych Grant N 1P03B01827.

1. Nelson R, Eisenberg D (2006) *Curr Opin Struct Biol* 16:260–265.
2. Tycko R (2000) *Curr Opin Struct Biol* 4:500–506.
3. Collins SR, Douglass A, Vale RD, Weissman JS (2004) *PLOS Biol* 2:1582–1590.
4. Dobson CM (2002) *Nature* 418:729–730.
5. Thirumalai D, Klimov DK, Dima RI (2003) *Curr Opin Struct Biol* 13:146–159.
6. Goldberg MS, Lansbury PT (2000) *Nat Cell Biol* 2:E115–E119.
7. Chen S, Ferrone FA, Wetzel R (2002) *Proc Natl Acad Sci USA* 99:11884–11889.
8. Petkova A, Leapman RD, Guo Z, Yau W, Mattson MP, Tycko R (2005) *Science* 307:262–265.
9. Hardy J, Selkoe DJ (2002) *Science* 297:353–356.
10. Prusiner SB (1998) *Proc Natl Acad Sci USA* 95:13363–13383.
11. Wetzel R (2002) *Structure (London)* 10:1031–1036.
12. Chan JC, Oyler NA, Yau WM, Tycko R (2005) *Biochemistry* 44:10669–10680.
13. Petkova AT, Ishii Y, Balbach J, Antzutkin O, Leapman R, Delaglio F, Tycko R (2002) *Proc Natl Acad Sci USA* 99:16742–16747.
14. Ma BY, Nussinov R (2002) *Proc Natl Acad Sci USA* 99:14126–14131.
15. Nelson R, Sawaya MR, Balbirnie M, Madsen A, Riekel C, Grothe R, Eisenberg D (2005) *Nature* 435:773–778.
16. Klimov DK, Thirumalai D (2003) *Structure (London)* 11:295–307.
17. Hwang W, Zhang S, Kamm RD, Karplus M (2004) *Proc Natl Acad Sci USA* 101:12916–12921.
18. Gnanakaran S, Nussinov R, Garcia AE (2006) *J Am Chem Soc* 128:2158–2159.
19. Gsponer J, Haberthur U, Caflisch A (2003) *Proc Natl Acad Sci USA* 100:5154–5159.
20. Straub JE, Guevara J, Huo SH, Lee JP (2002) *Acc Chem Res* 35:473–481.
21. Urbanc B, Cruz L, Ding F, Sammond D, Khare S, Buldyrev SV, Stanley H, Dokholyan NV (2004) *Biophys J* 87:2310–2321.
22. Klimov DK, Straub JE, Thirumalai D (2004) *Proc Natl Acad Sci USA* 101:14760–14765.
23. Buchete NV, Tycko R, Hummer G (2005) *J Mol Biol* 353:804–821.
24. Tarus B, Straub JE, Thirumalai D (2005) *J Mol Biol* 345:1141–1156.
25. Cannon MJ, Williams AD, Wetzel R, Myszka DG (2004) *Anal Biochem* 328:67–75.
26. Esler WP, Stimson ER, Jennings JM, Vinters HV, Ghilardi JR, Lee JP, Mantyh PW, Maggio JE (2000) *Biochemistry* 39:6288–6295.
27. Massi F, Straub JE (2001) *Proteins* 42:217–229.
28. Dima RI, Thirumalai D (2002) *Prot Sci* 11:1036–1049.
29. Socci ND, Onuchic JN, Wolynes PG (1996) *J Chem Phys* 104:5860–5868.
30. Stan G, Brooks BR, Thirumalai D (2005) *J Mol Biol* 350:817–829.
31. Thirumalai D, Hyeon C (2005) *Biochemistry* 44:4957–4970.
32. Lee JP, Stimson RR, Ghilardi JR, Mantyh PW, Lu YA, Felix AM, Llanos W, Behbin A, Cummings M, Criekinge MV, *et al.* (1995) *Biochemistry* 34:5191–5200.
33. van Gunsteren W, Billeter SR, Eising AA, Hünenberger PH, Krüger P, Mark AE, Scott W, Tironi I (1996) *Biomolecular Simulation: The GROMOS96 Manual and User Guide* (Vdf Hochschulverlag AG an der ETH, Zurich).
34. Berendsen HJC, Postma J, van Gunsteren W, Hermans J (1996) *Intermolecular Forces* (Reidel, Dordrecht, The Netherlands).
35. Ichiye T, Karplus M (1991) *Proteins* 11:205–217.
36. Kitao A, Hirata F, Go N (1991) *Chem Phys* 158:447–472.
37. Garcia AE (1992) *Phys Rev Lett* 68:2696–2699.
38. Amadei A, Linssen A, Berendsen H (1993) *Proteins* 17:412–425.
39. Mu Y, Nguyen P, Stock G (2005) *Proteins* 58:45–52.
40. Nguyen P, Stock G, Mittag G, Hu E, Li MS (2005) *Proteins* 61:795–808.
41. Cecchini M, Rao F, Seeber M, Caflisch A (2004) *J Chem Phys* 121:10748–10756.